LA-UR- 02-6790

Title: FROM SHOCK RESPONSE SPECTRUM TO TEMPORAL MOMENTS AND VICE-VERSA (U)

Author(s): François M. Hemez, LANL

Scott W. Doebling, LANL

Submitted to: For submission to the Journal of Sound and Vibration, November 2002.

FROM SHOCK RESPONSE SPECTRUM TO TEMPORAL MOMENTS AND VICE-VERSA

François M. Hemez[1], Scott W. Doebling[2]

Engineering Sciences and Applications (ESA-WR)

Los Alamos National Laboratory, P.O. Box 1663, Mail Stop P946

Los Alamos, New Mexico 87545, U.S.A.

ABSTRACT

Temporal moments have been used in engineering mechanics to condense the information contained in the shock response spectrum into a few scalar quantities. This paper presents an application of temporal moments to the propagation of an explosive-driven shock wave through an assembly of metallic parts. For this particular application, it is shown that temporal moments characterize the response of the system better than other features traditionally used in the analysis of nonlinear, transient events, such as the peak response or 10% duration of event. The inverse problem is also illustrated: the original, time-domain signals and their shock response spectra can be reconstructed from the temporal moments. This property makes temporal moments features of choice for the analysis of experimental data or the development of numerical models because they are low-dimensional quantities; they capture transient dynamics well; and they can be used to re-generate the original time signals (i.e. no information is lost in the feature extraction).

1. INTRODUCTION

Engineering analysis of complicated systems requires that features be extracted from the time domain or frequency domain responses. A feature is defined in this context as a low-dimensional quantity that captures the important characteristics of a signal in the time and/or frequency domains. Modal parameters have typically been used to define such quantities for linear systems. Other features encountered in engineering analysis are peak responses, damping coefficients, statistical moments and damage indicators. Temporal moments have also been proposed in the context of fast transients such as pyrotechnic shocks.[1, 2] Temporal moments are similar to statistical moments, and are computed from the square quantities $(y(t))^2$ where $y(t)$ represents the signal in the time domain.

[1] Technical Staff Member, ***hemez@lanl.gov***, 505-663-5204 (Voice), 505-663-5225 (Fax).
[2] Validation Methods Team Leader, ***doebling@lanl.gov***, 505-667-6950 (Voice), 505-665-2137 (Fax).

This publication has been approved for unlimited, public release on October 29, 2002. LA-UR-02-6790. Unclassified.

This publication discusses the application of temporal moments to characterize the shock response of a complex threaded assembly of components. The structure investigated is an assembly composed of several materials (titanium, aluminum, stainless steel) and several types of joints (threaded connection, bolted connection, tape joint). Four tests, labeled test 1 through test 4, have been performed by detonating patches of high explosives on the external surface of the system. For the purpose of this work, three tests can be considered replicates of each other (tests 1, 2 and 4) and the third test features a different assembly tolerance. Components of the three replicate tests are tightly assembled together while a small free-play is introduced between one component and the main thread prior to the third test. Acceleration responses are measured at six locations inside the system. Modal tests have also been performed even though the event of interest is a high frequency, nonlinear shock. Modal analysis shows that the system responds in the 20,000 to 50,000 Hertz range, which makes it somewhat difficult to excite the modes of interest. The shock response spectrum is therefore used for analyzing the response. This information is condensed further into three scalar numbers using the temporal moments. Additional information about the system, the tests performed and the numerical model developed can be found in References.[3, 4]

One objective of the analysis is to identify low-dimensional features capable of discriminating the loose assembly test (test 3) from the tight assembly tests (1, 2 and 4). The second objective is to demonstrate that reproducing a few low-dimensional features (i.e. the temporal moments) is equivalent to reproducing the original time series. These objectives are achieved by applying the procedure defined by Smallwood.[1] Random signals are generated that possess specific temporal moments and frequency content. It is then shown with a Monte Carlo simulation that the Fourier transforms, shock response spectra and temporal moments of these stochastic realizations converge asymptotically to the target values. The significance of this result is that analysts can focus their attention (development and validation of computational models, test-analysis correlation, model updating, etc.) on a few, low-dimensional features instead of the entire time series with minimum loss of information. In addition, the procedure can be applied to a wide range of stochastic and nonlinear signals.

2. DESCRIPTION OF THE EXPERIMENTS

The case study of interest in this paper is the propagation of a short-duration (micro-second) impulse across a threaded interface between metallic parts. The system is a connection known as a “manufacturing joint” where two cylindrical parts are connected via a titanium threaded shell part. Two mass simulators are attached to the central mount. They represent components of the assembly that are to be monitored for shock response. Because of the complex nature of the actual structural system and the inability to obtain a genuine article for what is a potentially destructive experiment, a surrogate assembly is devised to isolate the mechanisms of interest for the scenario. Validation of the response of

this assembly under a surrogate-loading environment is used to gain insight into modeling the fundamental mechanisms that influence the response of the actual system.

2.1 Hardware

The surrogate assembly is shown in Figure 1. Figure 2 illustrates a cross-section of the detail surrounding the manufacturing joint. The finite element model is developed to predict the response of the system in configurations that cannot be tested experimentally. Reference 5 discusses the modeling, which will not be addressed here.

The components consist of the bell-shaped titanium (Ti) “mount”; two aluminum (Al) shells, the “upper shell” that is cylindrical, and the lower shell, that is cylindrical with a “flare” at the bottom edge; and two mass simulators, a conical aluminum mass referred to as the “upper mass” and a cylindrical steel mass referred to as the “lower mass” (not pictured).

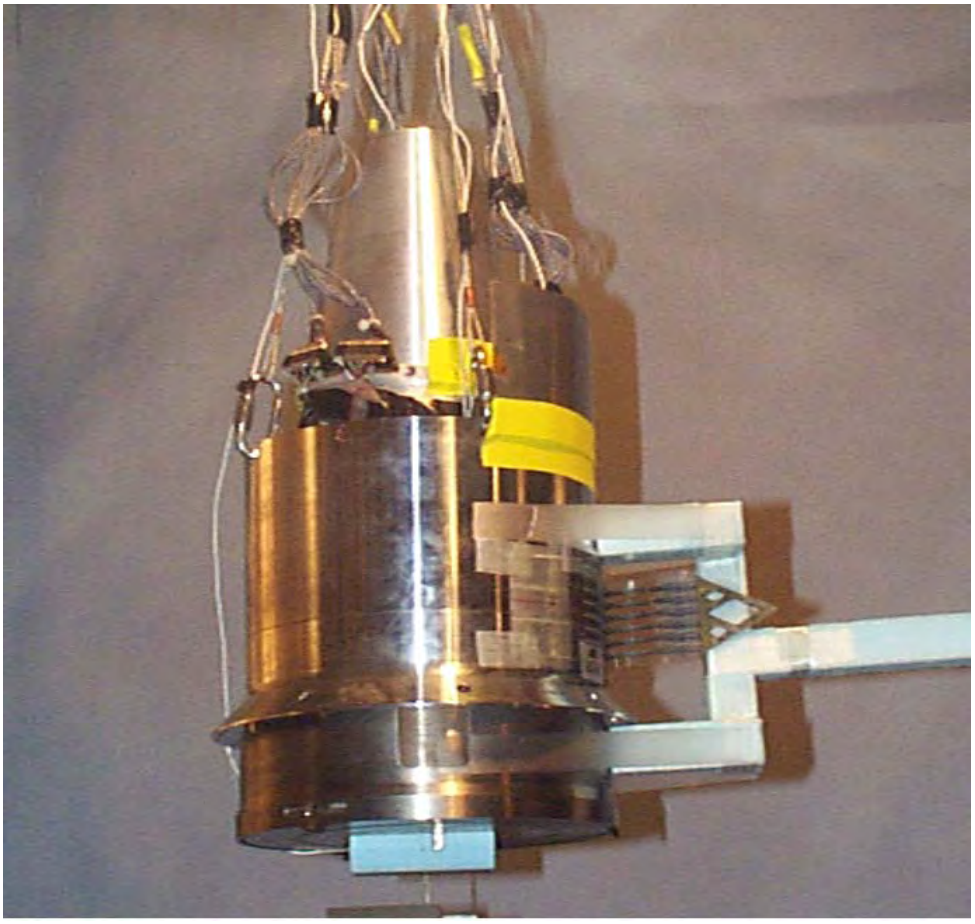

Figure 1. Experimental hardware.

The upper mass simulator bolts onto foot-like appendages on top of the mount. The lower mass simulator is inserted into the bell end of the mount and held in place with a device known as a "tape joint" that essentially consists of two wedges of metal driven into a slot in the mount.[6] Also, a ring-shaped threaded titanium nut is used to hold the lower shell into place on the mount (see Figure 2).

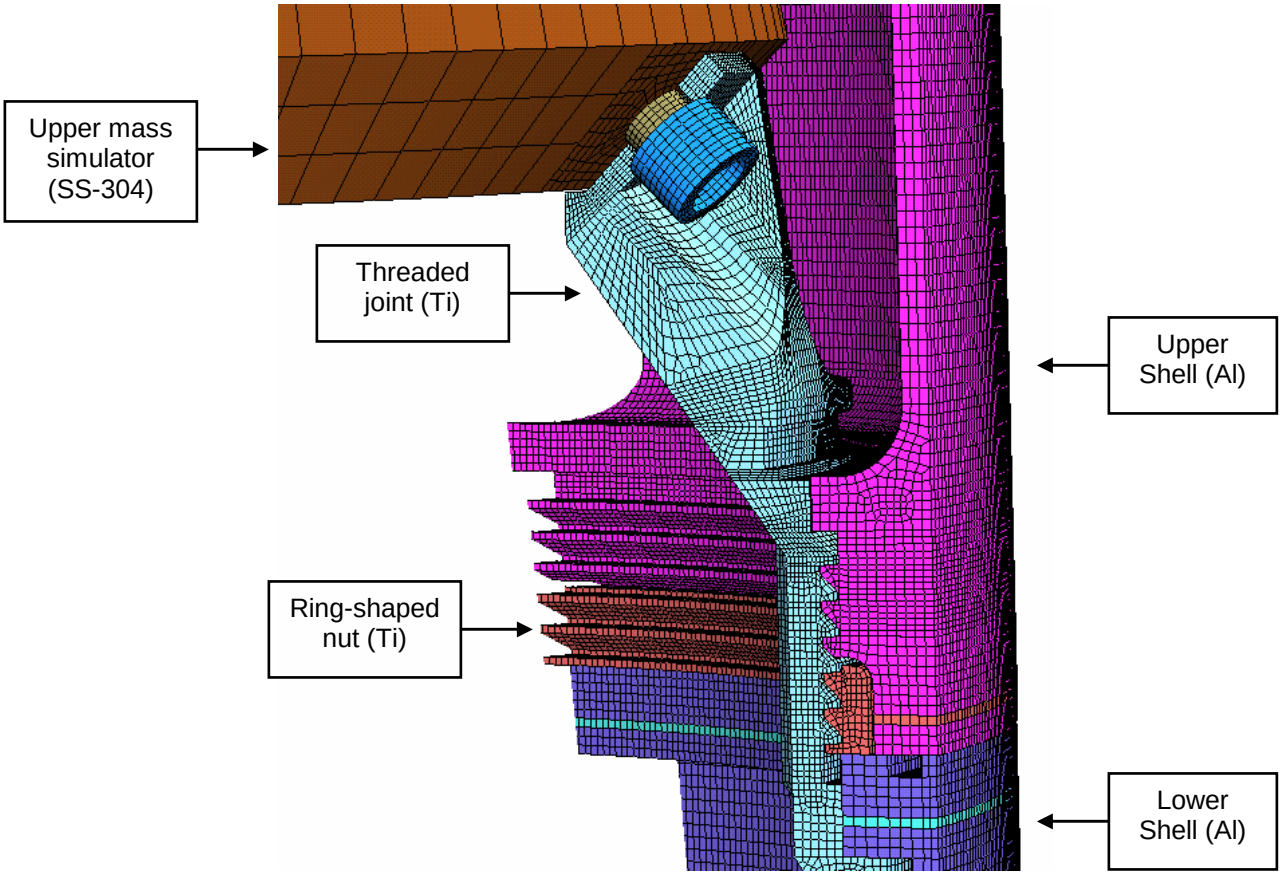

Figure 2. Detail of the threaded joint.

Analyzing the system through either experimental measurements or numerical simulations proves to be quite challenging because of the complexity of the geometry, the number of different material interfaces (Al/Ti, Al/SS-304, Ti/Ti, Ti/SS-304) and the variability introduced during assembly.

2.2 Instrumentation

The threaded assembly was instrumented with thirty-three strain gages attached to the inside surface of the titanium mount. The strain gages provided data on the localized propagation of the shock around the circumference of the mount. The strain gages had an active length of 0.8 mm to obtain localized effects. One of the strain gages was found to be faulty during the pre-test check of the sensors.

In addition, six accelerometers (Endevco 7270A-200k, 1mV/g) were used to instrument the acceleration response of the mass simulators. They were located on either end of both payload mass simulators. Four were oriented laterally in the direction of the delivered impulse and two were oriented along the axis of the structure, see Figure 3.

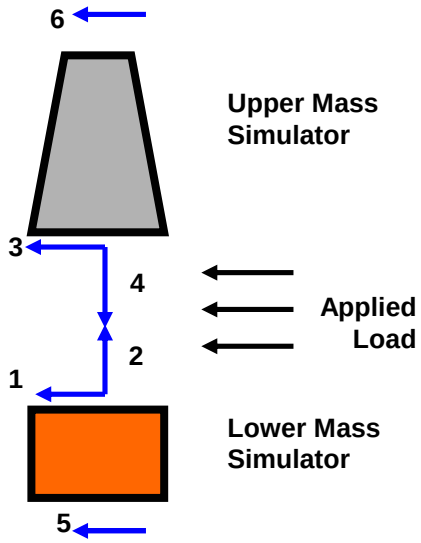

Figure 3. Location of Accelerometers.

The conditioned strain signals had a frequency response bandwidth of 100 kHz and the accelerometer signals had a frequency response of 500 kHz. This study is restricted to acceleration responses collected at sensors 5 and 6 because they are important for the analysis and offer the best signal-to-noise ratios.

2.3 Explosive Source

Extensive research was performed to determine the impulse-loading configuration. Design requirements were that the pressure peak at the surface of the threaded assembly be less than 5 kbar with an impulse between 2 and 4 ktaps.

The design requirements were met by interfacing the sheet explosive with a buffer layer. A neoprene buffer was chosen such that the resulting pressures fit within the design requirements. The low-level impulse was achieved by cutting the sheet into strips and spacing them out over the target area. Figure 4 shows that the pressure load applied directly under a strip is very similar to the load applied between two strips, therefore, verifying our computational load model. Figure 4 also shows that the pressure history is a short-duration event (1.8 micro-second), therefore, providing a good realization of an impulse excitation.

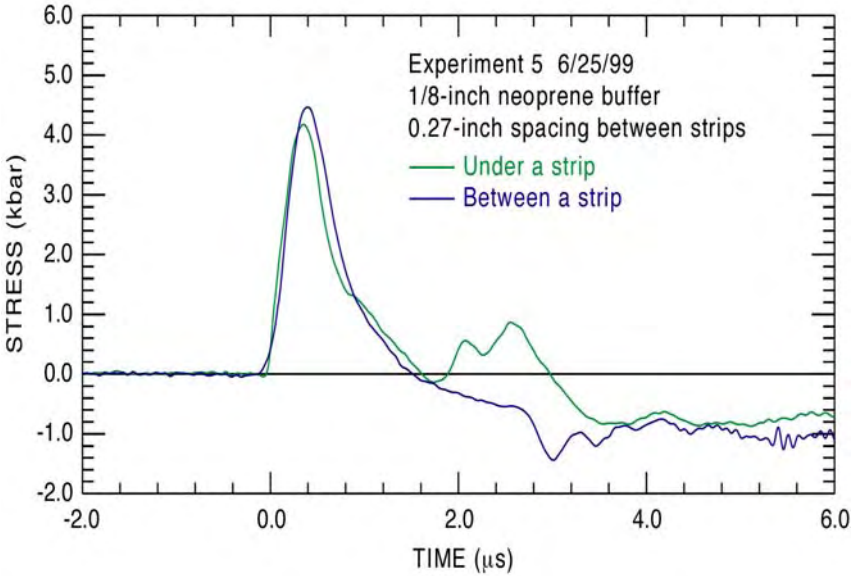

Figure 4. Measured pressure history.

2.4 Test Matrix

A suite of four tests was conducted in July 1999. Additional testing will be conducted in the year 2003. Two experimental factors were studied in this test suite, the manufacturing tolerance for the aluminum shells and an assembly tolerance.

Two sizes of Al shells were manufactured, one with nominal clearances (the "loose" set) and one with smaller than nominal clearances (the "tight" set). The assembly tolerance relates to how much radial clearance is allowed between the lower shell and the mount directly behind the location of the explosive charge. Figure 5 illustrates the assembly tolerance or "gap" that can be opened or closed when the components are assembled.

Table 1. Experimental test matrix.

		Assembly	
		Loose	*Tight*
Manufacturing	*Loose*	Test 3	Tests 1&2
	Tight		Test 4

The combinations of these factors for each test are shown in Table 1. Tests 1 and 2 were repeated tests intended to give a bound for the test-to-test repeatability. However, the structure for test 1 was assembled at Los Alamos and shipped for testing, while test units 2, 3, and 4 were all assembled and

tested by the same team. The shipping of test unit 1 could have allowed for the preloads to be released, causing some significant differences between units 1 and 2. For this reason, the results of test 1 are not discussed here.

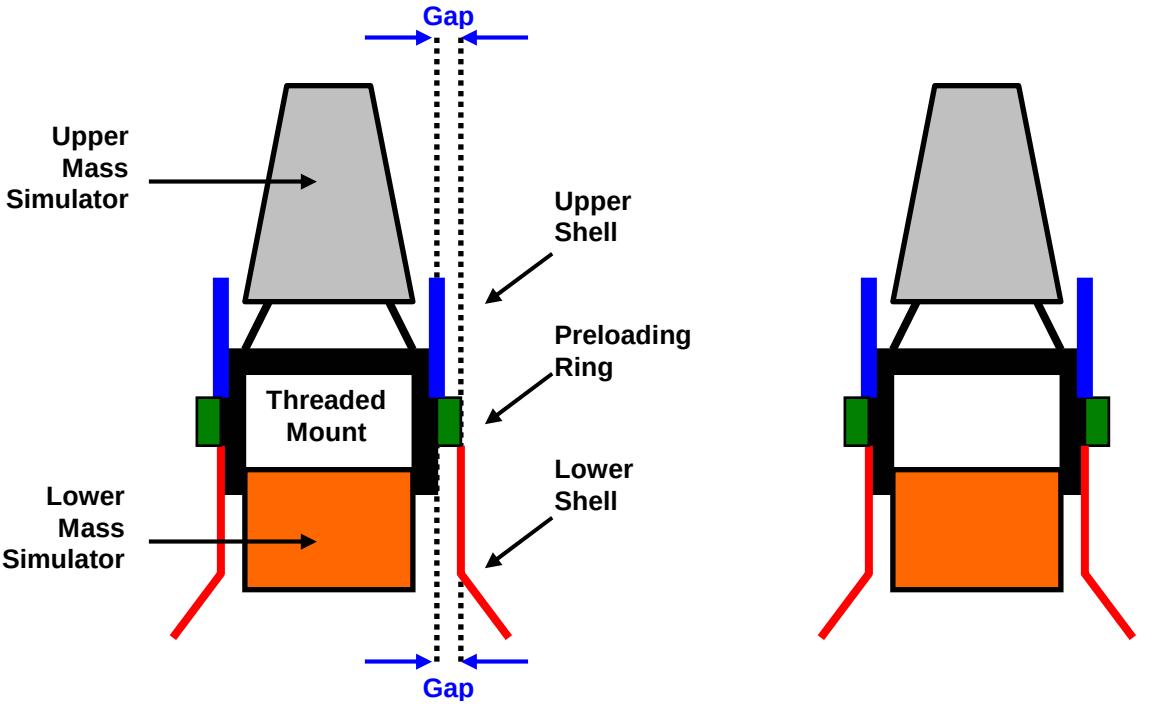

(a) Configuration with an assembly gap. *(b) Configuration without a gap.*

Figure 5. Definition of the assembly tolerance.

Also, variation of the manufacturing tolerance did not influence the measured dynamics significantly. In the remainder, test units 2 and 4 are considered to be replicates. The first question that this work addresses is therefore to identify low-dimensional features that can be applied to the analysis of non-linear, transient dynamics and capable of discriminating test 3 (loose assembly) from tests 2 and 4 (tight assembly).

2.5 Experimental Results

For the impulse experiments, the test article was suspended using wire rope to create a pendulum with a length of about 1 m, see Figure 1. Pendulum motion was monitored with a fiber optic displacement sensor to determine the total impulse delivered to the tests article. Total impulse values measured for the four tests are listed in Table 2.

For each experiment, new upper and lower aluminum shells were used to ensure that accumulated damage did not affect test results. A raw sample time history for the response accelerometer 6 and test unit 4 is shown in Figure 6. The data cleansing (decimating, filtering) is discussed briefly in section 4.

Table 2. Measured impulse values.

Test Unit	Total Impulse ($\times 10^{+3}$ N*sec.)	Total Impulse (lbf*sec.)
1	103.7 +/- 4.4	0.233 +/- 0.01
2	113.8 +/- 4.4	0.256 +/- 0.01
3	108.0 +/- 4.4	0.243 +/- 0.01
4	103.7 +/- 4.4	0.233 +/- 0.01

(Note: 1 dyne = 10^{-5} Newton = 2.25 10^{-6} lbf.)

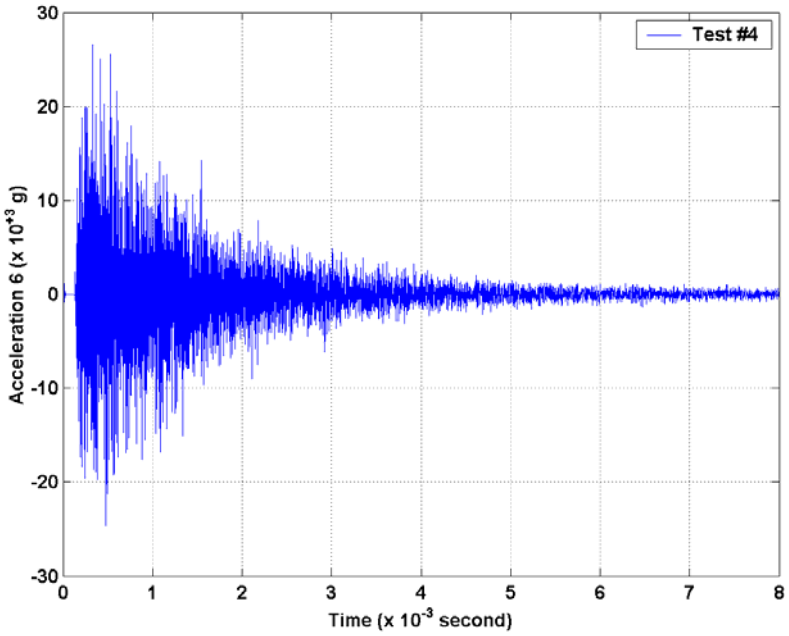

Figure 6. Acceleration response (sensor 6, test 4).

3. OBJECTIVES

As mentioned previously, this work focuses on tests 2, 3, 4 and acceleration responses collected at sensors 5 and 6. The objectives are stated below:

- ***Survey the existing features for non-linear, transient dynamics***. Can the information such as the acceleration in Figure 6 be characterized by a few, low-dimensional numbers?

- ***Investigate the discriminating power of features for our application***. Can features be found that would the tests performed? Specifically, can test 3 (loose assembly) be discriminated from tests 2 and 4 (tight assembly)?

- ***Investigate the usefulness for inverse problem solving***. Assume that the features extracted from two signals are similar. To which extent are the original signals also similar?

The third objective addresses the feasibility of transforming features back into time-domain signals. Such transformation is generally not possible because an infinite number of signals can exhibit the same feature value. This is the case of features such as the peak response or the exponential damping coefficient. With temporal moments, however, a mechanism is available to generate time series from the features and frequency-domain information.

For the threaded assembly application, acceleration time histories $y_e(t)$ will be generated from the knowledge of temporal moment values. It will then be verified that the realizations $y_e(t)$ converge to the signals $y(t)$ from which the temporal moments were originally extracted, see section 8.

4. DATA CLEANSING

In this section, the data cleansing procedure is briefly described. Data cleansing is aimed, essentially, at filtering out unwanted dynamics from the measured response. It is also designed to produce data sets that exhibit the same time-frequency properties and biases (in terms of sampling, aliasing, etc.) as the responses predicted by the finite element model.

The response of the system is analyzed from 0.115 to 2.415 milliseconds (ms) to avoid including in the time signals an early event due to the electrical impulse of the explosive's detonation. The period analyzed therefore consists of 2.3 ms of data. Signals are decimated by a factor 5 to obtain an effective sampling rate of 200 kHertz. An 8^{th}-order Butterworth low-pass filter is applied with cut-off frequency at 50 kHertz. Finally, the signals are normalized by the total impulse of each test (see Table 2) and the mean of each processed signal is removed.

The processed signals are pictured in Figure 7 (sensor 5 on the lower mass) and Figure 8 (sensor 6 on the upper mass) for each one of the four test units.

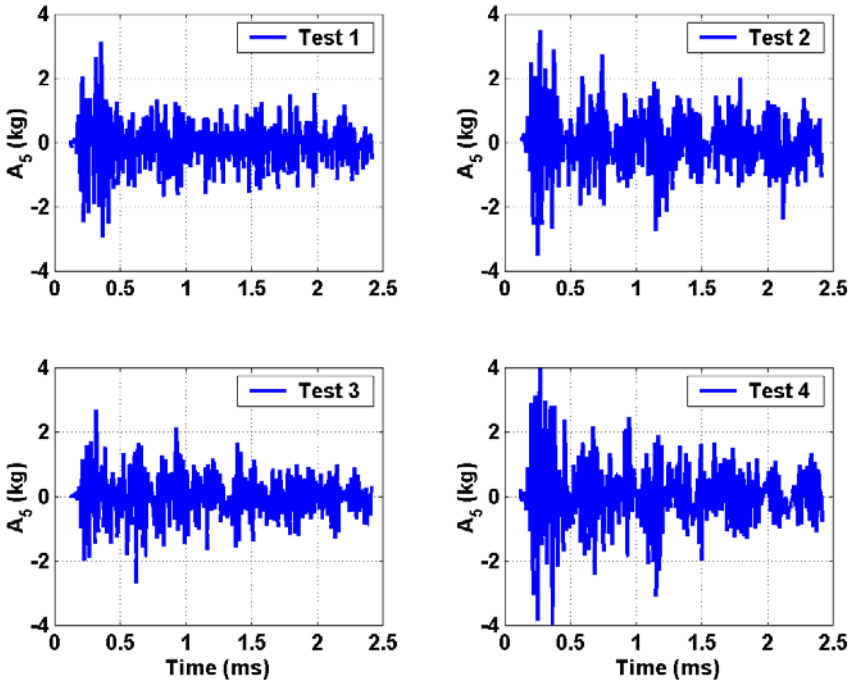

Figure 7. Processed accelerations at sensor 5.

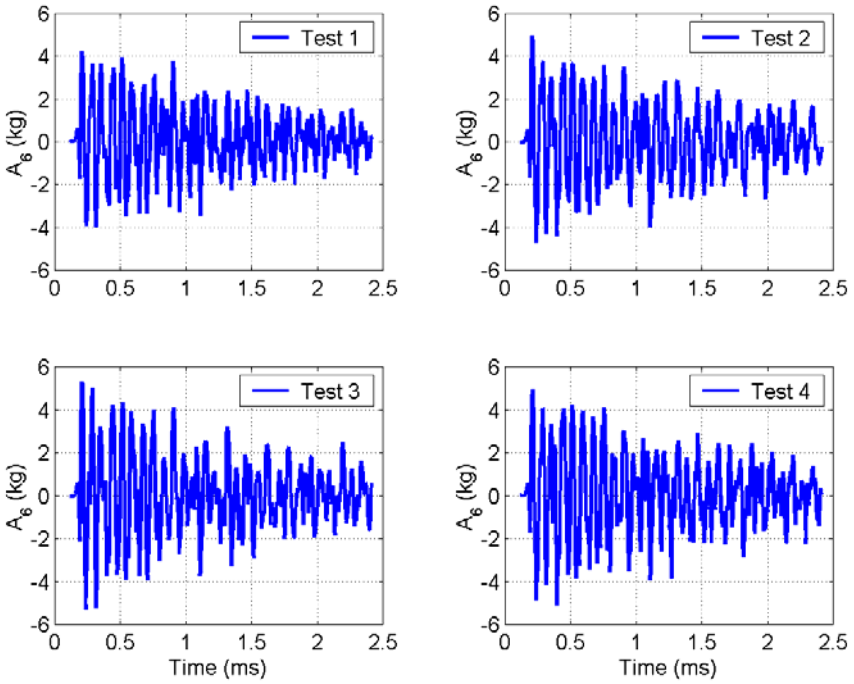

Figure 8. Processed accelerations at sensor 6.

5. FEATURES FOR TRANSIENT EVENTS

When it comes to the analysis of transient events, modal analysis is generally not appropriate. This is because the dynamics of interest is high frequency, while modal superposition is most appropriate to identify low-frequency dynamics. Also, non-linearity might manifest itself in the response (energy coupling, bifurcation and chaos are well-known examples), making it questionable to calculate Fourier transforms or power spectral density estimates. Therefore, features such as resonant frequencies and modal damping ratios cannot be used to characterize the response of the threaded joint.

The state-of-the-practice for analyzing waveforms of transient events relies on the following features:

- ***Peak values***. Peaks include absolute peak values and ranges, that is, the difference between maximum and minimum values.

- ***10% duration of the event***. This feature is defined as the time between the instant of peak response (for example, shock arrival) and the instant that the waveform has decayed to 10% of its peak.[2]

- ***Exponential decrement***. This feature is defined as the scalar exponent *d* of an exponential decay $z(t)=Ae^{-dt}$ best-fitted to the response *y(t)*.

- ***Statistical moments***. A probability density function and statistics can be estimated from the signal, as it is assumed to represent realizations of a random variable.

- ***Principal Component Decomposition (PCD)***. The PCD is also referred to as the Karhunen-Loëve decomposition or principal orthogonal modes. It generalizes the notion of modal superposition to non-linear systems and has been applied to test-analysis correlation and model updating.[7, 8]

- ***Fractal dimensions***. Fractal analysis characterizes the "growth" of the signal in time as a function of various wavelengths or time scales. Numerous fractal dimensions are defined, that include the Holder exponent, Lyapunov exponent and the Higuchi dimension.[9]

- ***Shock response spectrum (SRS)***. The SRS simulates the response "seen" by a single degree-of-freedom system that would be subjected to the transient waveform (section 6).

- ***Temporal moments***. Temporal moments are scalar quantities that condense the information of the SRS. Computing temporal moments is analogous to the calculation of the statistical moments of a random variable (section 7).

For example, features advocated by NASA for the analysis of pyro-shock events (such as lift-off or stage separation) include the peak value, the 10% duration of the event and the shock response spectrum.[2] The above list is not meant to be exhaustive, nor does it represent a rigorous literature review.

All the features cited above are evaluated with the data sets collected. For the sake of conciseness, the numerical results are not detailed here. Suffices to say that, with the exception of the SRS and temporal moments addressed in sections 6 and 7, none of the features provide a clear discrimination between the responses of test unit 3 and test units 2 and 4.

Specific difficulties associated with the forward problem include the fact that the first three types of features (peak value, 10% duration of the event and exponential decrement) provide no clear discrimination between the three tests. The same conclusion is reached with statistical moments. The PCD generates several important modes, which indicates that the response is dynamically rich. The main limitation of the PCD, however, is that modal pairing through correlation leads to inconclusive results. Finally, fractal analysis has no inherent physical interpretation with respect to the mechanical response of the structure.

6. THE SHOCK RESPONSE SPECTRUM

The Shock Response Spectrum (SRS) synthesizes the response of a single degree-of-freedom mass-spring-damper *(m; k; c)* oscillator to a transient event. It calculates the vibration environment "seen" by the oscillator due to the transient waveform. The SRS is extensively used to design, test and qualify equipments to shock environments because it represents the response that a piece of equipment mounted at that location on the structure would experience.

Figure 9 illustrates the SRS calculation. The transient waveform is applied to a moving base, either as a force as pictured in Figure 9 or as an acceleration signal. The response *x(t)* is obtained by integrating the equation of motion:

$$m\ddot{x}(t) + c\dot{x}(t) + kx(t) = f(t) \tag{1}$$

for a specific combination of mass *m*, stiffness *k* and damping *c* values. Then, the solution *x(t)* is reduced to a single number, for example, the RMS displacement or the peak acceleration. The procedure is

repeated for different values of the triplet *(m; k; c)* and results are displayed as the curve of design values (for example, peak acceleration values) versus triplets *(m; k; c)*.

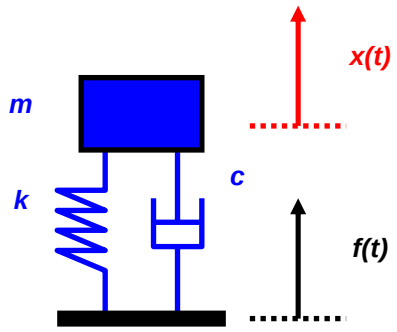

Figure 9. Calculation of the SRS.

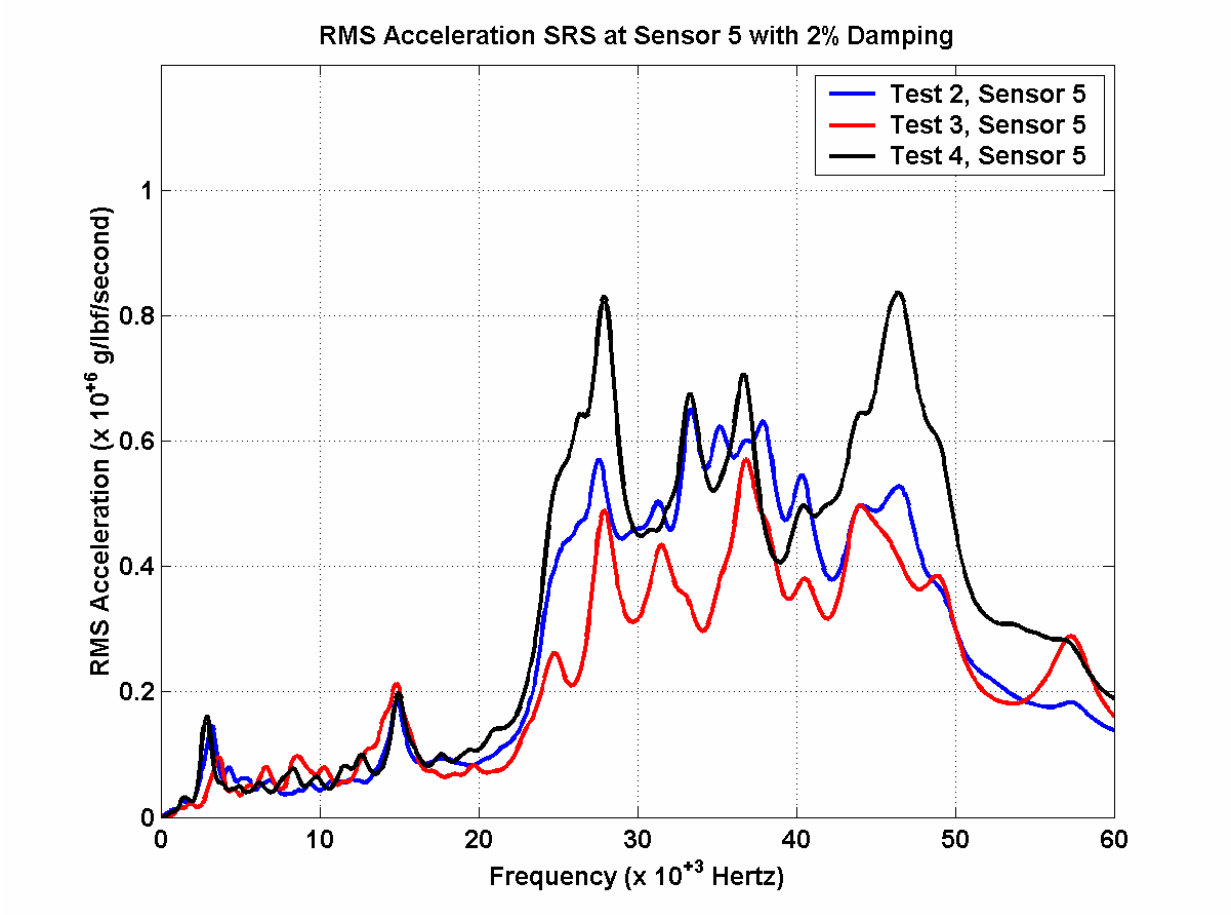

Figure 10. Shock response spectra at sensor 5.

Figures 10 and 11 show the spectra of RMS accelerations at sensors 5 and 6 for tests 2-4. The frequency—which is the square root of (*k/m)*—is varied from DC to 60 kHertz while the damping

coefficient *c* is kept constant and equal to 2% modal damping. There is no particular reason for selecting this damping value, except that it is, according to many experimentalists, representative of the analysis.

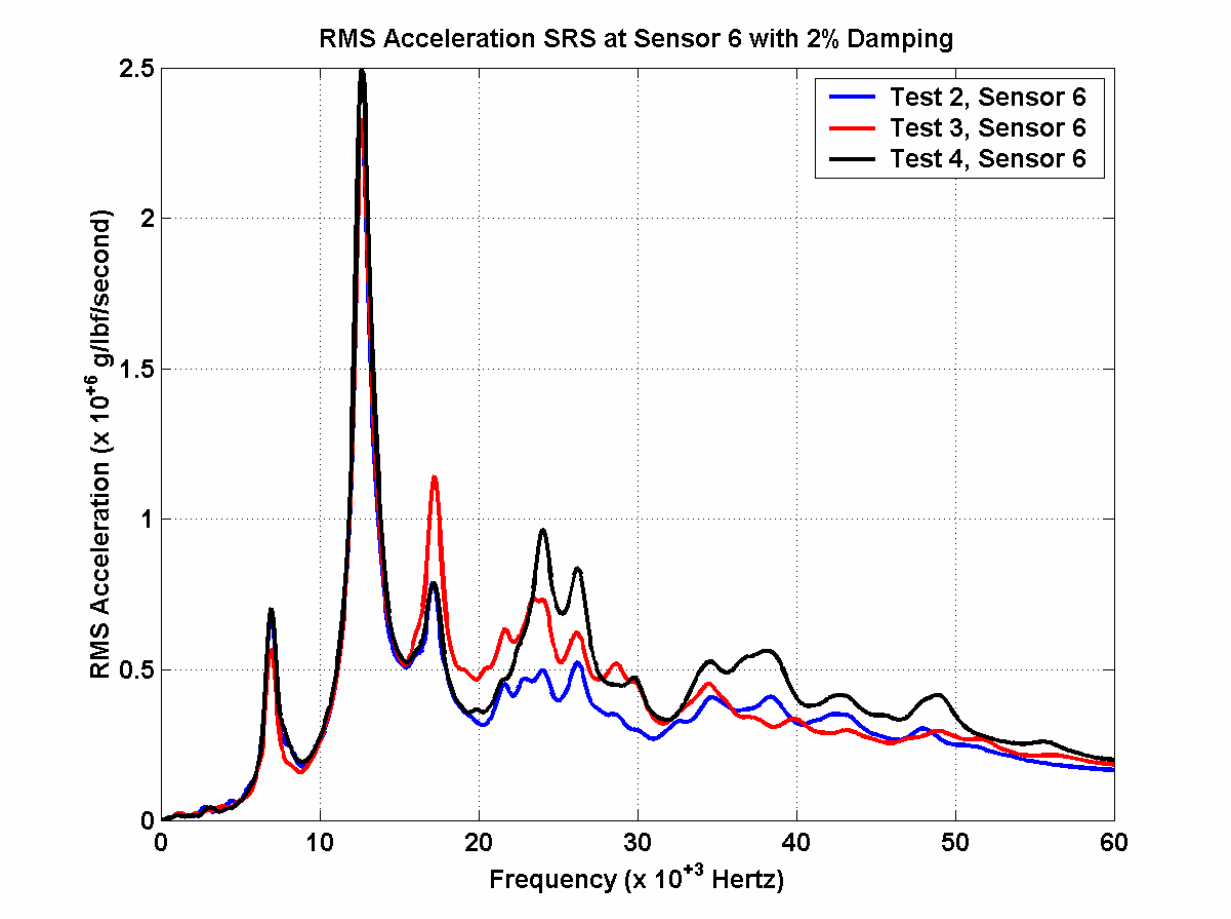

Figure 11. Shock response spectra at sensor 6.

Table 3. Cumulated RMS acceleration.

Test Unit	Area of SRS (Sensor 5)	Area of SRS (Sensor 6)
2	70.91	91.35
3	56.42	96.57
4	78.69	101.99

(Units: x 10^{+6} g/lbf/second.)

In Figures 10 and 11, the SRS provides valuable information about the energy content "seen" by sensors 5 and 6. Most of the energy that reaches sensor 5 is above 25 kHertz, while most of the energy that reaches sensor 6 is below 20 kHertz. Test 3 produces a significantly different SRS signature at sensor 5 (lower mass). It suggests that the presence of an assembly gap during the test redirects some of

the energy away from the lower mass simulator. This analysis is summarized in Table 3 that lists the cumulated RMS accelerations, that is, the areas under the SRS curves.

Advantages of the SRS include very minimal assumptions. The SRS can be defined and computed for linear or non-linear systems alike, stationary or non-stationary signals. Limitations are that the SRS provides no information about the duration of the transient, distribution of energy in time and oscillatory nature of the waveform.

7. TEMPORAL MOMENTS

First, the temporal moments are defined. Their physical meaning is briefly discussed in section 7.2. Lastly, they are applied to the analysis of the threaded assembly experiment (section 7.3).

7.1 Temporal Moments

The temporal moments $M_i(t_s)$ are calculated as weighted summations of the time signals squared:

$$M_i(t_s) = \int_{-\infty}^{+\infty} (t - t_s)^i \left(y(t)\right)^2 dt \tag{2}$$

where t_s denotes a shift in time and the subscript "*i*" represents the moment's order. For simplicity, the temporal moments are denoted M_i when the time shift is set to zero (t_s=*0*).

The temporal moments $M_i(t_s)$ can be normalized to generate what is referred to in the literature as the central moments.[1, 10] Central moments are computed as shown in equation (3) and defined in Table 4.

$$\begin{cases} E = M_o, \quad A_e^2 = \dfrac{E}{D}, \quad T = \dfrac{M_1}{M_o}, \quad D^2 = \dfrac{M_2}{M_o} - \left(\dfrac{M_1}{M_o}\right)^2 \\ S_t^3 = \left(\dfrac{M_3}{M_o}\right) - 3\left(\dfrac{M_1 M_2}{M_o^2}\right) + 2\left(\dfrac{M_1}{M_o}\right)^3, \quad S = \dfrac{S_t}{D} \\ K_t^4 = \left(\dfrac{M_4}{M_o}\right) - 4\left(\dfrac{M_1 M_3}{M_o^2}\right) + 6\left(\dfrac{M_1^2 M_2}{M_o^3}\right) - 3\left(\dfrac{M_1}{M_o}\right)^4, \quad K = \dfrac{K_t}{D} \end{cases} \tag{3}$$

Equations (2-3) show that computing temporal moments from time signals is straightforward. Practical considerations include the fact that the waveform must be truncated as it reaches the noise floor.

Small signal values away from the time origin (or centroïd) can result in large errors in the moment estimates. Mitigation measures include truncation or applying an exponentially decaying window.

Table 4. Definition of central moments.

Symbol	Definition	Units
E	Energy	$(EU)^2$*Second
A_e	Root energy amplitude	(EU)
T	Central time (centroïd)	Second
D	RMS duration	Second
S_t	Central skewness	Second
S	Normalized skewness	Unitless
K_t	Central kurtosis	Second
K	Normalized kurtosis	Unitless

(EI: Engineering unit in which $y(t)$ is expressed.)

Band-limited temporal moments have also been proposed to analyze the signals in specific frequency bands.[10] The estimation of band-limited temporal moments is constrained by the so-called "uncertainty principle". Essentially, if the transient is short duration, then the resolution in the frequency domain cannot at the same time be narrow. Requiring a higher time resolution is only possible at the expense of the frequency resolution, and vice-versa.

7.2 Physical Interpretation

Clearly, the first central moment E represents the total "energy" of the signal. It is also equal to the value of the auto-correlation function R_{yy} at zero delay. The root energy amplitude A_e represents the signal's overall amplitude. It differs from E by a normalization factor equal to the inverse of a "characteristic duration" D.

The central time T, or centroïd, is defined as the time index t_s that produces a zero first moment, that is, t_s such that $M_1(t_s)$=0. Looking at the distribution of energy in time, T represents the "equilibrium point", that is, the instant where half of the energy has already passed and half has yet to arrive at the sensor.

The root mean square duration D describes the dispersion of the waveform. A rule-of-thumb is that the significant part of the transient's energy should be within 2 or 3 RMS durations around the centroïd T. It is analogous to a standard deviation in statistics.

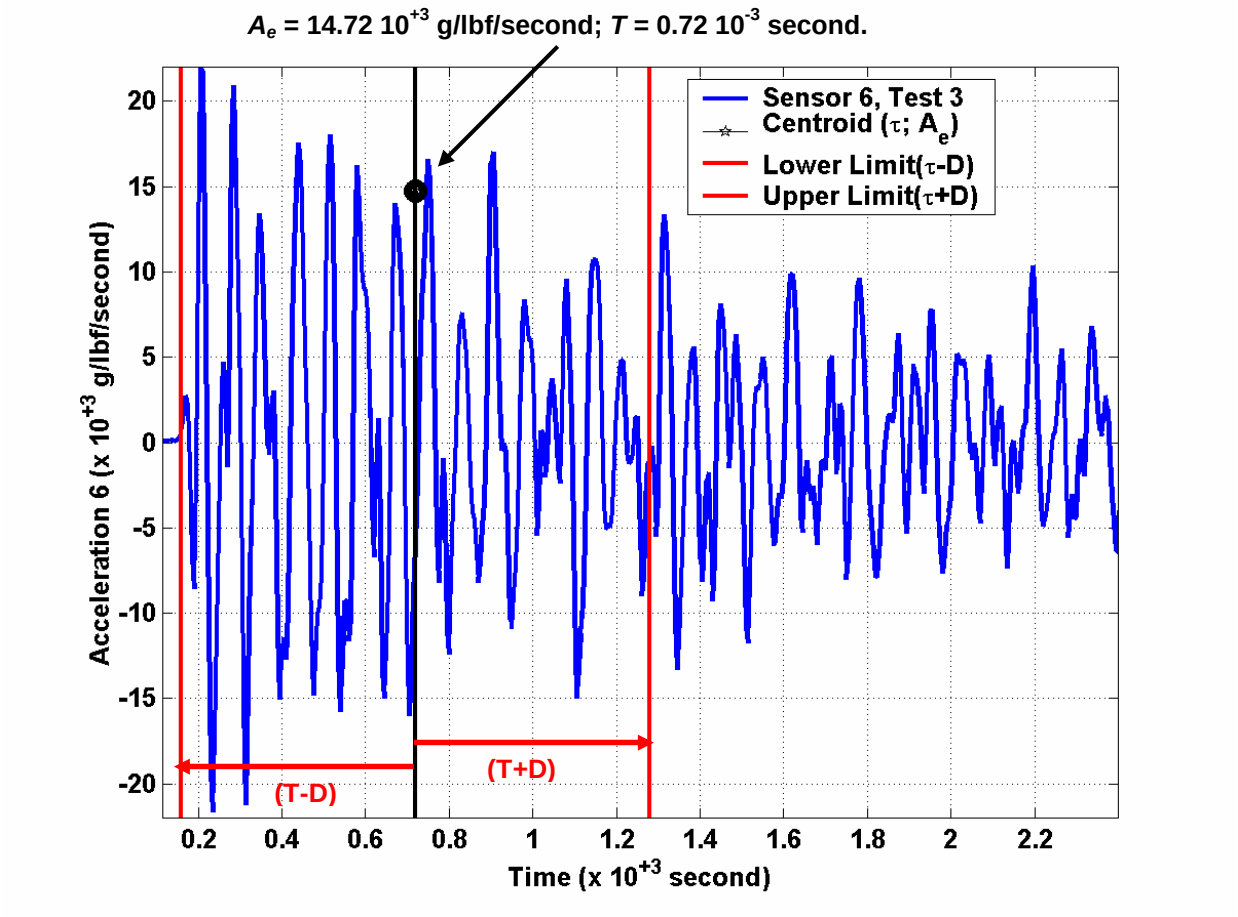

Figure 12. Illustration of temporal moments.

Figure 12 compares the central moments A_e, T and D to the acceleration signal at sensor 6, test unit 3 to illustrate their physical meaning.

When the energy of the signal is not centered symmetrically about the centroïd T, the central skewness S_t indicates the direction of the asymmetry. But it does not, as sometimes mentioned, measure the rise time or fall time. Positive skewness indicates a waveform that has high amplitudes before the centroïd and a long low-amplitude tail. Negative skewness is the opposite.

The kurtosis K_t—together with the skewness S_t—can be useful for characterizing waveforms whose envelopes are not unimodal. Large kurtosis values often indicate multi-modal responses.

7.3 Application to the Threaded Joint

Tables 5 and 6 list the central moments E, T, D, S_t and K_t at sensors 5 and 6, respectively. The immediate observation is that the open-gap configuration of test unit 3 redirects the energy away from the

lower mass simulator, as shown by the low energy value *E* at sensor 5. If anything, some of the redirected energy reaches the upper mass simulator sooner because the central time *T=0.72* ms at sensor 6 is the lowest of the three tests. The overall waveform does not change significantly, as indicated by the relative stability of central moments *D*, S_t and K_t.

Table 5. Central moments at sensor 5.

Symbol	Test 2	Test 3	Test 4
E (10^{+3} g^2/lbf^2/sec.)	31.00	**19.59**	43.89
T (10^{-3} sec.)	0.86	0.87	0.71
D (10^{-3} sec.)	0.66	0.60	0.60
$\boldsymbol{S_t}$ (10^{-3} sec.)	0.53	0.51	0.58
$\boldsymbol{K_t}$ (10^{-3} sec.)	0.79	0.74	0.77

Table 6. Central moments at sensor 6.

Symbol	Test 2	Test 3	Test 4
E (10^{+3} g^2/lbf^2/sec.)	105.35	121.29	135.49
T (10^{-3} sec.)	0.77	**0.72**	0.73
D (10^{-3} sec.)	0.57	0.56	0.55
$\boldsymbol{S_t}$ (10^{-3} sec.)	0.52	0.55	0.54
$\boldsymbol{K_t}$ (10^{-3} sec.)	0.72	0.74	0.72

In summary, it can be concluded that the temporal moment analysis is successful at discriminating test 3 from the others. Even though the variations of *T*, *D*, S_t and K_t are not statistically significant—they vary by less than twice the standard deviation, less energy reaches sensor 5 with the loose assembly tolerance. Energy also tends to be "seen" sooner at sensor 6. This conclusion must however be considered with caution because only two replicate tests are currently available. As mentioned previously, more testing is being scheduled to better study the experiment's variability more thoroughly.

8. RECONSTRUCTING TIME SIGNALS

After having investigated the forward problem of feature extraction (from time series to features), the inverse problem is now discussed. We would like to answer the following question:

"If a model predicts given temporal moments values, to which extent are the original time series reproduced as well?"

Clearly, answering such question requires a procedure to generate time series—that may include random components—that possess specific moment values. Inverting the feature extraction transform is made possible using Smallwood's "product model".[1] An illustration of the procedure defined to "draw" stochastic time series with specific temporal moments and time-frequency properties is provided in sections 8.1 to 8.4. Section 8.5 presents a Monte Carlo simulation that illustrates the asymptotic convergence.

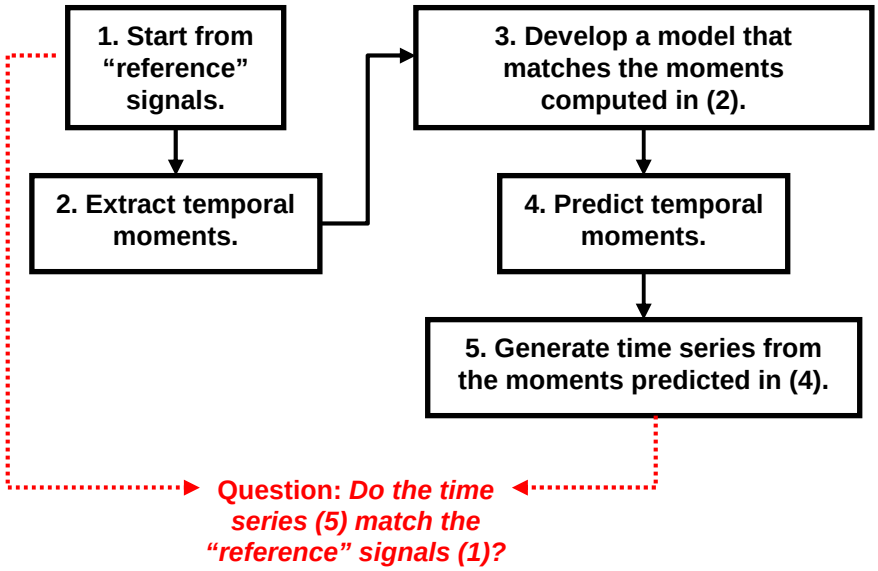

Figure 10. Verifying that matching temporal moments is equivalent to matching time series.

Figure 10 illustrates the verification that matching the temporal moments is equivalent, at least in the asymptotical sense, to matching the time signals.

8.1 The Product Model

In References 1 and 10, Smallwood advocates to represent transients as the combination of a mean response, an energy spectrum and temporal moments.

The mean response characterizes any deterministic component of the signal. It also describes the basic shape of the waveform. The energy spectrum characterizes how the energy is distributed in frequency. Possible choices are the Fourier spectrum, the power spectral density or the SRS. Temporal moments provide additional information about the overall energy content, time-of-arrival, spread of the signal in time and shape of the waveform (depending on which are included).

This representation is called the "product model" and captured mathematically by equation:

$$y(t) = y_m(t) + \sum_{b=1...N_b} W_b(t) g_b(t) \tag{4}$$

where:

- ***$y_m(t)$: Deterministic, mean signal***. It represents, for example, the mean of a collection of signals. In the application presented, the mean component is removed, yielding $y_m(t)=0$.

- ***$W_b(t)$: Deterministic, parameterized window***. The window's parameters can be selected such that the temporal moments of $W_b(t)$ in the bandwidth of interest are equal to the band-limited moments of the original signal $y(t)$. The terminology "time window" refers in this context to a deterministic, time-domain waveform of specific shape.

- ***$g_b(t)$: Realization of a band-limited, stationary, Gaussian process***. The random process has a zero mean and unit variance. Realizations can be obtained that have the same energy spectrum as the original signal in the bandwidth of interest.

The summation in equation (4) represents a superposition of time domain signals constructed in different frequency bands. The application presented in sections 8.3 to 8.5 assumes that a single bandwidth is defined from 0-to-60 kHertz. With multiple bandwidths, the procedure below is repeated over every band.

8.2 General Procedure

The "trick" introduced by the decomposition (4) is that features of the windows $W_b(t)$, such as temporal moments, can be constrained independently of time-frequency properties.

The procedure defined to reconstruct time signals from temporal moments follows. First, it is assumed that the signal possesses a random component and can be represented by the product model (4). The windows $W_b(t)$ are defined such that their temporal moments in the bandwidth of interest are equal to the band-limited temporal moments of the target waveform $y(t)$. Section 8.3 shows how to generate time windows with specific temporal moments.

Next, realizations of the random process $g_b(t)$ are computed and constrained to feature the same energy spectrum (for example, the same Fourier spectrum) in the bandwidth of interest as the target

waveform *y(t)*. Section 8.4 shows how to draw samples of a stationary, Gaussian process that exhibits a specific frequency spectrum.

Finally, the contributions $W_b(t)$ and $g_b(t)$ are assembled according to the product model (4) and, possibly, over multiple frequency bands. Although no formal proof of convergence is established, section 8.5 illustrates that Monte Carlo simulations provide signals whose average properties (such as temporal moments, Fourier transform and SRS) match the properties of the target signal *y(t)*.

8.3 Window Selection and Optimization

Several candidate windows can be proposed. Clearly, the shape of the window must match the shape of the waveform to capture. Windows found in the literature include:

$$\begin{cases} W_b(t) = A\left(t^n - T^{(n-p)}t^p\right) \text{ with } p > n \\ W_b(t) = At^n e^{-at} \\ W_b(t) = A\left(e^{-at} - e^{-bt}\right) \end{cases} \tag{5}$$

Smallwood, for example, presents applications using the first family of windows in equation (5).[1] Once a family of parameterized windows has been selected, its parameters are optimized to match target values of *E*, *T*, *D*, S_t and K_t. In some cases, it may happen that the temporal moments can be analytically computed as functions of the window's parameters.

Table 7. Optimized moments at sensor 6, test 3.

Symbol	Target	Obtained	Error
E (10^{+3} $g^2/lbf^2/sec.$)	121.29	121.29	0.0%
T (10^{-3} sec.)	0.72	0.72	0.0%
D (10^{-3} sec.)	0.56	0.56	0.0%
$\boldsymbol{S_t}$ (10^{-3} sec.)	0.55	0.54	2.6%
$\boldsymbol{K_t}$ (10^{-3} sec.)	0.74	0.73	1.3%

In the threaded joint application, the last family of windows (5) is selected. The three central moments *E*, *T* and *D* (sensor 6, test 3) are matched by optimizing the parameters *(A; a; b)*. The objective function is the RMS error between the moments *E*, *T* and *D* of a window $W_b(t)$ and the target moments of test unit 3's response *y(t)* at sensor 6. Table 7 compares the target and optimized temporal moments. Note that S_t and

K_t are reproduced as well, even though they were not used to define the objective function during the optimization of the window's parameters.

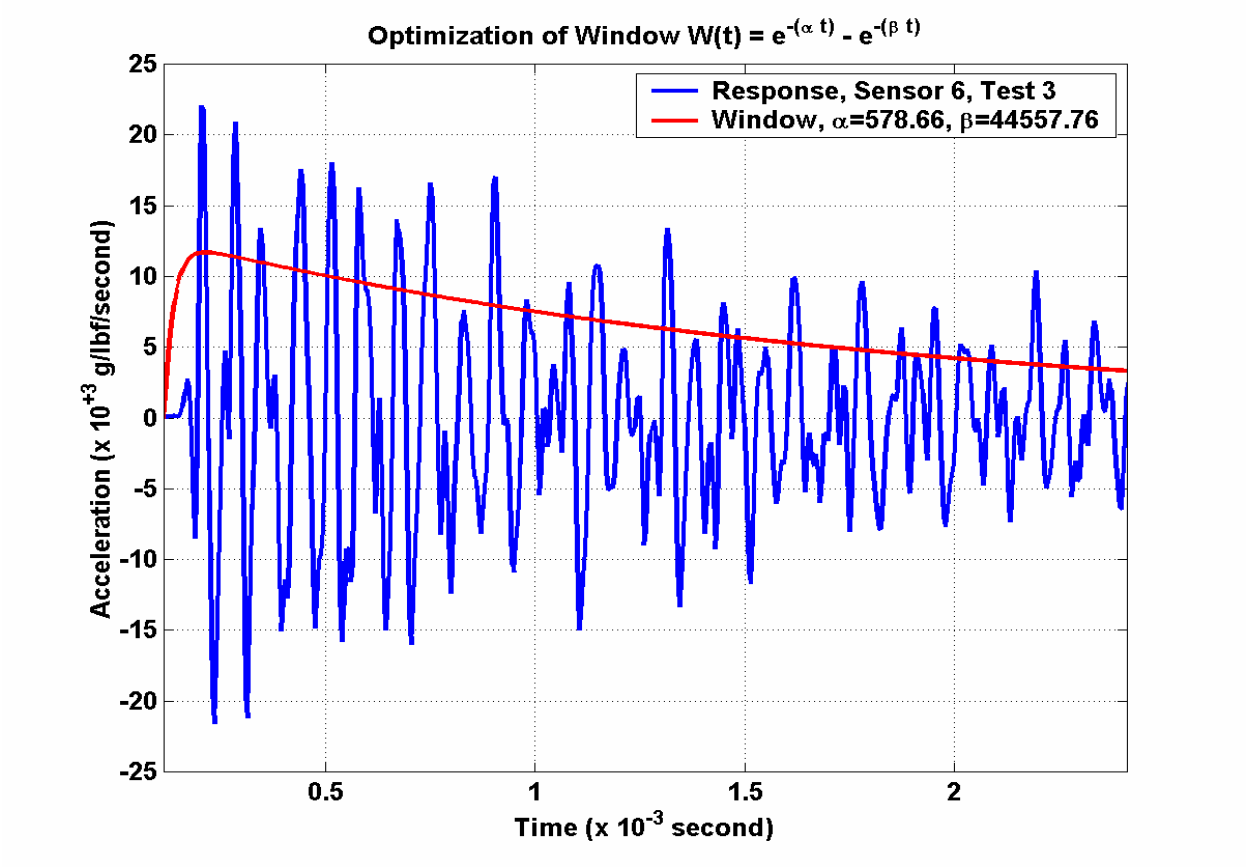

Figure 13. Window $W_b(t)$ and target signal.

Figure 13 compares the final window $W_b(t)$ to the signal $y(t)$ that we are trying to reproduce. It shows that the overall RMS amplitude and shape of the window are representative of the signal's own. Once optimized, the window remains unchanged for the remainder of the analysis. In a band-limited analysis, the procedure is the same with one window defined per bandwidth.

8.4 Realization of Random Processes

Next, realizations of a stationary, Gaussian process are constructed. The energy spectrum of processes $g_b(t)$ is set to a target spectrum. Here, the Fourier spectrum $G(s)$ of the target signal $y(t)$ is chosen. This information is combined to a random phase $P(s)$. Realizations of the process $g_b(t)$ are obtained by inverse-Fourier transforming the resulting quantity:

$$g_b(t) = \int_0^{s_{max}} \left(G(s) e^{jP(s)} \right) e^{jst} ds \tag{6}$$

where s_{max} denotes the maximum frequency of the bandwidth of interest. A Matlab™-based algorithm implemented to generate realizations $g_b(t)$ is provided in the Appendix.

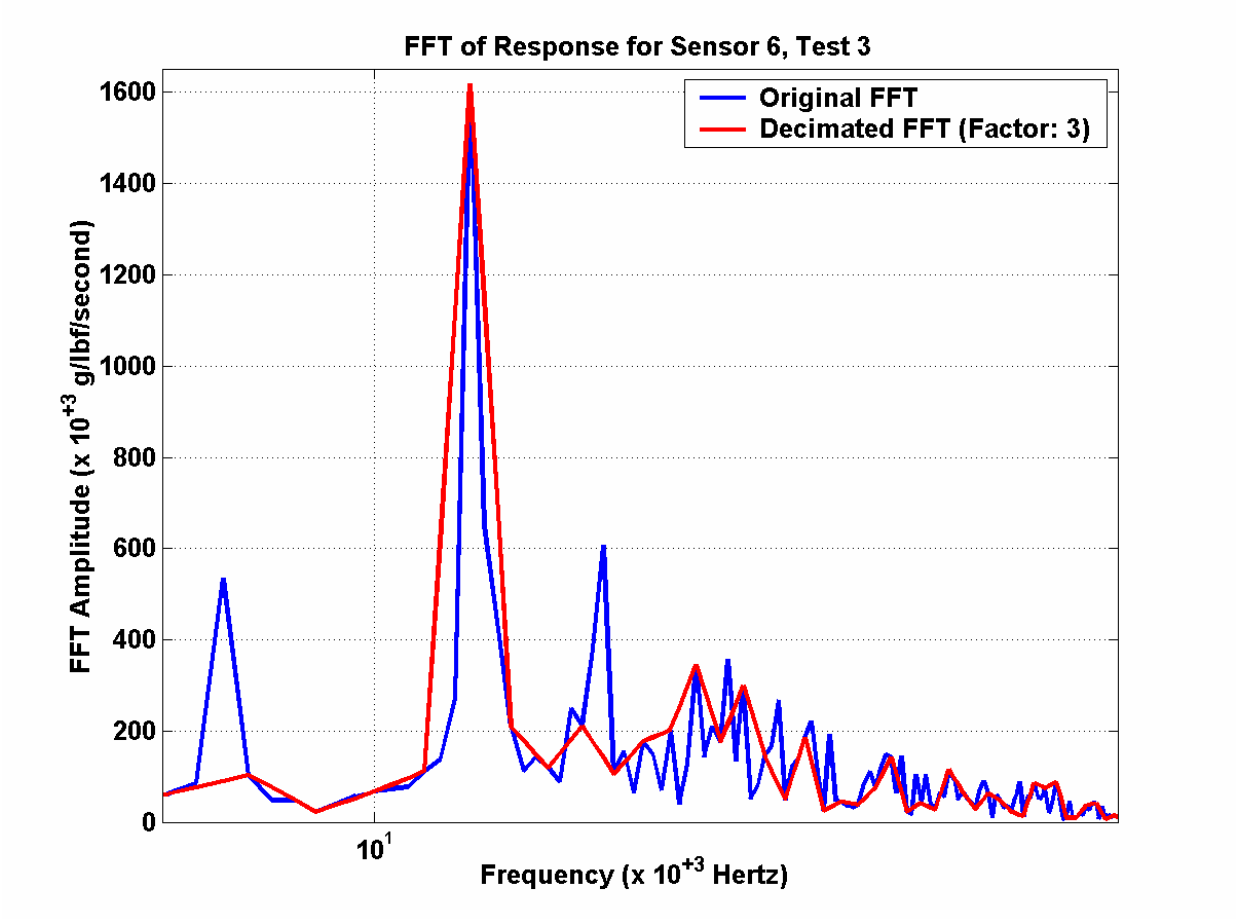

Figure 14. Decimated Fourier transform *G(s)*.

Figure 14 shows the frequency spectrum *G(s)* used in equation (6). It is obtained by decimating the Fourier transform of the original signal *y(t)* at sensor 6, test unit 3. Decimation (here, by a factor 3) reduces the total amount of information stored. Missing some of the peaks does not deteriorate too adversely the quality of the final estimates of *y(t)*, as shown in section 8.5.

Figure 15 compares a signal $y_e(t)=W_b(t)g_b(t)$ generated by the method aforementioned to the measurement at sensor 6, test unit 3. Clearly, the characteristics of the original signal *y(t)* (amplitude, frequency content and energy dissipation) are reproduced by the surrogate $y_e(t)=W_b(t)g_b(t)$.

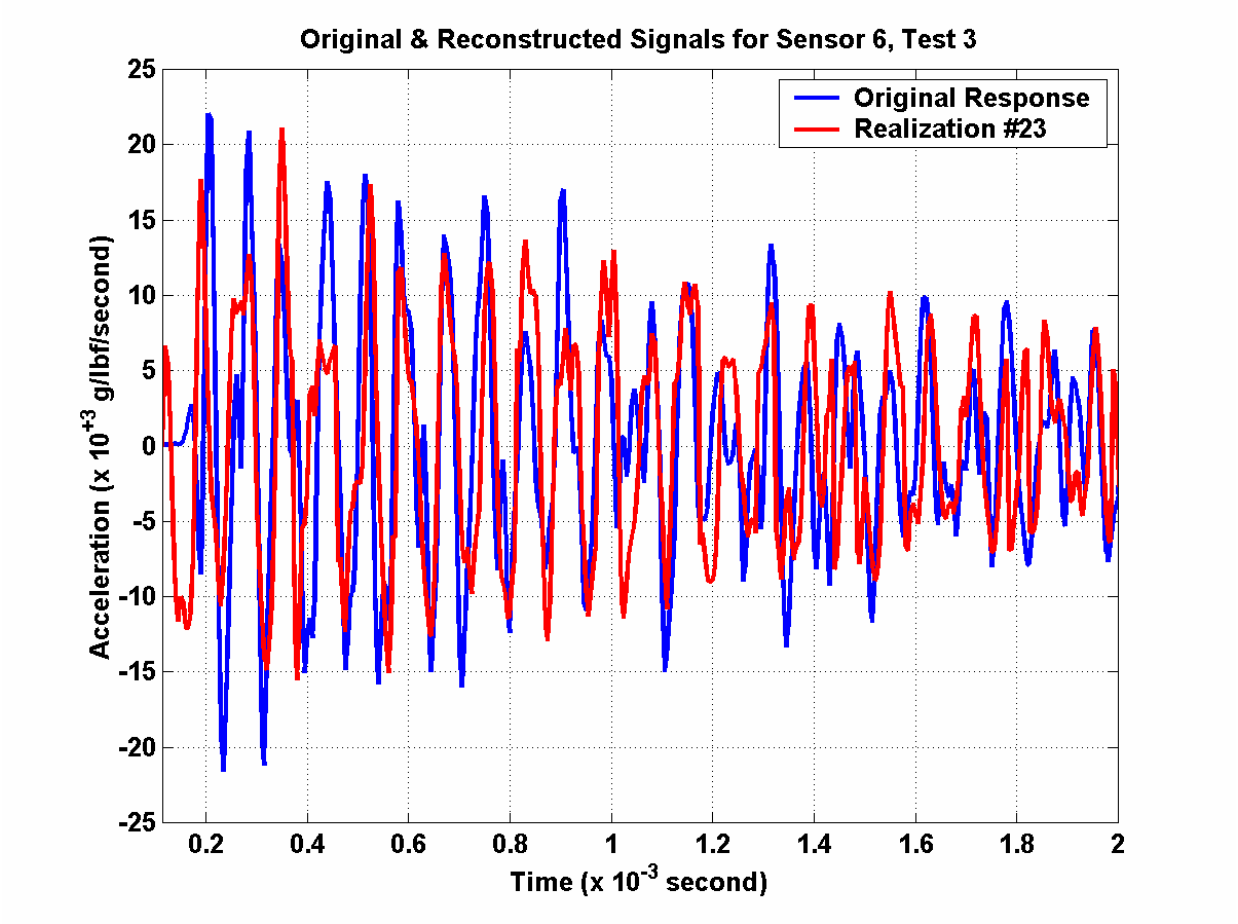

Figure 15. Comparison of synthesized signal $y_e(t)$ and original signal $y(t)$.

Of course, inverse-Fourier transforming the spectrum $G(s)$ of Figure 14 would return the original signal $y(t)$ because the Fourier transform is invertible. However, this defines a deterministic transform that cannot account for the stochastic nature of the signal. The procedure based on the product model, on the other hand, offers the possibility to generate ***stochastic*** signals with specific temporal moments, damping characteristics and frequency content.

8.5 Results of a Monte Carlo Simulation

Finally, the results of a Monte Carlo simulation are presented. The simulation consists of drawing 1,000 realizations $g_b^{(k)}(t)$ and calculating the resulting time series $y_e^{(k)}(t)=W_b(t)g_b^{(k)}(t)$. What plays the role of the "random variable" in this Monte Carlo simulation is the stochastic realization $g_b(t)$ or more precisely, as will be explained below, its phase information. Windows $W_b(t)$, once they have been optimized to match the target temporal moments, stay unchanged in each bandwidth. The thousand signals $y_e^{(1)}(t)$ … $y_e^{(1,000)}(t)$ are averaged into an estimate $y_e(t)$ of the measured signal $y(t)$ at sensor 6, test unit 3.

Table 8 compares the temporal moments of the estimate $y_e(t)$ and the true moments extracted from the measurements $y(t)$. Moments E, T and D are obtained within 1.5% of the target values. The skewness and kurtosis are also accurate given the fact that the window $W_b(t)$ has not been optimized to account for S_t and K_t.

Table 8. Moments of the mean signal $y_e(t)$ at sensor 6, test 3.

Symbol	Target	Obtained	Error
$\boldsymbol{E}$ (10^{+3} g^2/lbf^2/sec.)	121.29	120.70	0.5%
$\boldsymbol{T}$ (10^{-3} sec.)	0.72	0.73	1.4%
$\boldsymbol{D}$ (10^{-3} sec.)	0.56	0.56	0.0%
$\boldsymbol{S_t}$ (10^{-3} sec.)	0.55	0.52	5.5%
$\boldsymbol{K_t}$ (10^{-3} sec.)	0.74	0.73	1.3%

Figures 16 and 17 compare the FFT and SRS spectra of the measured signal $y(t)$ to those of the reconstruction $y_e(t)$. The 1,000 realizations are averaged and shown in red, solid lines. Also shown in black, solid lines are the 68% confidence intervals (mean plus or minus one standard deviation).

In both cases, the true spectrum is contained within plus or minus one standard deviation of the mean. Figure 16 does not come as a surprise because the Fourier transform is enforced through the realization of processes $g_b(t)$. No information, however, about the SRS is explicitly provided, yet, the agreement with measured data shown in Figure 17 is excellent.

This illustration does not constitute a formal proof of convergence but it seems to indicate that the time-frequency properties of the estimate $y_e(t)$ converge rapidly to those of the measured signal.

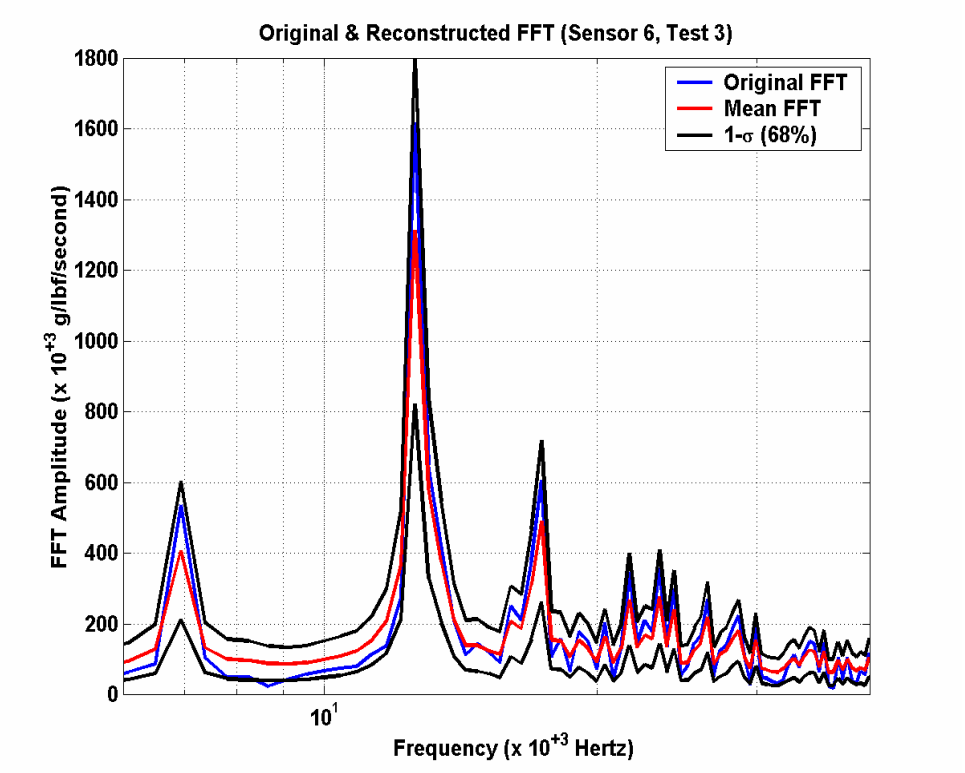

Figure 16. Synthesized and original FFT.

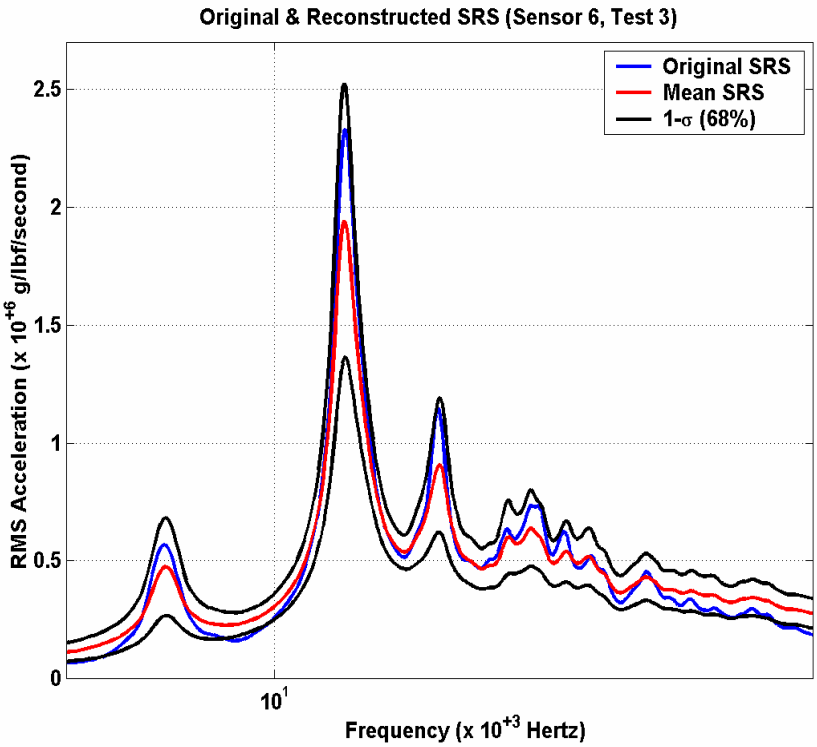

Figure 17. Synthesized and original SRS.

9. CONCLUSION

An application of temporal moments to the characterization of a transient event is presented. It is found that the temporal moments perform better than other low-dimensional features when it comes to discriminate tests associated with different assembly tolerances.

This investigation attempts to highlight the many advantages of temporal moments for the analysis of non-linear, stochastic responses:

- ***Usefulness for testing***: Smallwood uses temporal moments to generate signals that define specific vibrating environments on shake tables.[11]

- ***Usefulness for correlation***: Comparing multi-dimensional responses is difficult and statistically meaningless unless large amounts of data are available. Temporal moments are easy to compare because of their low dimensionality.

- ***Usefulness for modeling***: Instead of developing numerical models that attempt to reproduce time series, models can be developed to predict the temporal moments. Then, a procedure has been demonstrated to generate signals from temporal moments that, asymptotically, possess the same time-frequency properties as the original signals.

It is the authors' opinion that the last point is critical when it comes to developing surrogate models or fast-running models, possibly for programming into on-board computing units. Instead of aiming at time series, surrogate models can be developed to reproduce temporal moments—which is much simpler and computationally efficient—with little loss of information because a procedure is available to synthesize the times series, if needed.

ACKNOWLEDGMENTS

The pyro-shock testing was designed and performed by SRI International, Menlo Park, California. The authors wish to express significant recognition to LANL staff Thomas A. Butler, Amy N. Robertson and graduate student Amanda L. Cundy (Virginia Tech University). The authors also thank David O. Smallwood from Sandia National Laboratories in Albuquerque, New Mexico for answering their questions and providing valuable guidance.

REFERENCES

[1]Smallwood, D.O., "Characterization and Simulation of Transient Vibrations Using Band Limited Moments," *Shock and Vibration*, Vol. 1, No. 6, 1994, pp. 507-527.

[2]Mulville, D.T., **Pyroshock Test Criteria, NASA Technical Standard**, *Report #NASA-STD-7003*, May 1999.

[3]Butler, T.A., Hemez, F.M., Schultze, J.F., Doebling, S.W., "Model Validation for a Complex Jointed Structure," *SEM IMAC-XIX*, Kissimmee, FL, Feb. 5-8, 2001, pp. 1318-1324.

[4]Groethe, M., "Manufacturing Joint Validation Tests," *Report #10129*, SRI International, Menlo Park, CA, Nov. 1999.

[5]Doebling, S.W., Hemez, F.M., Schultze, J.F., "Validation of the Transient Structural Response of a Threaded Assembly," *4th AIAA Non-Deterministic Approaches Forum*, Denver, CO, Apr. 22-25, 2002.

[6]Robertson, A.N. (Editor), Doebling, S.W., Hemez, F.M., Maupin, R., Butler, T.A., Schultze, J.F., Cundy, A.L. (Contributors), "Validation of the Transient Structural Response of a Threaded Assembly," *Internal Report*, Los Alamos National Laboratory, Los Alamos, New Mexico, October 2002, *in preparation*.

[7]Lenaerts, V., Kerschen, G., Golinval, J.C., "Parameter Identification of Nonlinear Mechanical Systems Using Proper Orthogonal Decomposition," *SEM IMAC-XVIII*, San Antonio, TX, Feb. 7-10, 2000, pp 133-139.

[8]Hasselman, T.K., Anderson, M.C., Wenshui, G., "Principal Components Analysis for Nonlinear Model Correlation, Updating and Uncertainty Evaluation," *SEM IMAC-XVI*, Santa Barbara, CA, Feb. 2-5, 1998, pp. 664-651.

[9]Simard, P., Le Tavernier, E., "Fractal Approach for Signal Processing and Application to the Diagnosis of Cavitation," *Mechanical Systems and Signal Processing*, Vol. 13, No. 3, May-June 2000, pp. 459-469.

[10]Smallwood, D.O., "Variance of Temporal Moment Estimates of a Squared Time History," *63rd Shock and Vibration Symposium*, Oct. 1992, pp. 389-399.

[11]Smallwood, D.O., "Time History Synthesis for Shock Testing on Shakers," *Seminar on Understanding Digital Control and Analysis in Vibration Test Systems*, Shock & Vibration Information Center, Navy Research Laboratory, Washington, D.C., May 1975, pp. 23-42.

APPENDIX. MATLAB™ CODE

The Fourier transform *G(s)* of a realization is obtained by combining a given frequency spectrum *G_a* with a random phase *G_p*. Then, the inverse Fourier transform of *G(s)* is calculated and transformed to a real-valued realization $g_b(t)$. In the following, *N* denotes the number of frequency bins and *W* denotes the optimized window $W_b(t)$.

```
% Generate a random phase of length N
>> G_p = pi*(2*rand(N,1)-1);
% Calculate G(s), the Fourier transform of g(t)
>> G = G_a.*exp(sqrt(-1).*G_p);
% Calculate the inverse Fourier transform of G(s)
>> iG = ifft(G);
% Convert to a real-valued signal g(t)
>> g = sign(cos(angle(iG))).*abs(iG);
% Normalize the signal g(t)
>> g_n = (1/std(g)).*(g-mean(g));
% Calculate the product model
>> y = y_mean + W.*g_n;
% End (or loop over the frequency bands)
```

Sent to:

Professor W. Soedel
Editor of the Journal of Sound and Vibration
School of Mechanical Engineering
Purdue University
1077 Ray W. Herrick Laboratories
West Lafayette, Indiana 47907-1077
Phone: (765) 494-8613; *Fax*: (765) 494-0787; *Email:* werner.soedel.1@purdue.edu